Low energy electron interactions with Iodine molecule (I_2)

Hitesh Yadav

Department of Physics, Sardar Patel University, Vallabh Vidyanagar,India

E-mail: hitesh0507@gmail.com

Minaxi Vinodkumar

Electronics Department, V.P. & R.P.T.P. Science College, Vallabh Vidyanagar,India

E-mail: minaxivinod@yahoo.co.in

Chetan Limbachiya

Department of Applied Physics, The M. S. University of Baroda, Vadodara,India

E-mail: cglimbachiya-apphy@msubaroda.ac.in

P.C. Vinodkumar

Department of Physics, Sardar Patel University, Vallabh Vidyanagar,India

E-mail: p.c.vinodkumar@gmail.com

N. J. Mason

School of Physical Sciences, University of Kent, UK

E-mail: N.J.Mason-OBE@kent.ac.uk

February 2014

Abstract. A theoretical analysis is performed for electron interactions with the Iodine molecule (I_2) for incident energies ranging from 0.1 eV to 20 eV. The calculations were carried out using Quantemol-N package, which uses the UK Molecular R-matrix Codes. Electron interactions with the I_2 molecule have been studied with several target models in its equilibrium geometry, and the results are reported for the optimized target model. Scattering calculations are performed to provide resonance parameters along with Dissociative Electron Attachment (DEA) Cross-Sections. In addition, the study also focussed on the estimation of various cross-sections such as elastic, electronic excitation, differential, momentum transfer, ionization and total cross-sections. Many of these cross-sections reported here are for the first time for electron interaction with the iodine molecule to the best of our knowledge.

1. Introduction

I_2 is one of the stable and less volatile molecule compared to other elements of the halogen series. It is also one of the most useful molecules of various applied interest [1, 2, 3, 4, 5, 6, 7, 8, 9]. In the study of atmospheric geochemistry and preventive methods for thyroid-based disorders are the most popular uses of iodine molecules [1, 10]. Technologically, iodine molecule is employed as one of the prompt applied molecule used in the numerical modelling of plasma kinetics [11, 12], wherein data on electron impact cross-sections of I_2 molecule are used as input parameters. In the absence of experimental data of electron impact ionisation cross-sections and electronic excitation cross-sections of I_2 molecule, the respective data of the atomic iodine are modified and employed in such studies [12]. Iodine is also being used as a molecular propellant in electrostatic plasma thrusters, such as Hall effect thrusters (HET) [13, 14, 15]. The electron impact inelastic data such as excitation, ionisation and dissociative electron attachments are used for the application of I_2 as a molecular propellant [13, 14, 15]. Thus, the electron impact study with I_2 molecule and estimation of various cross-sections become more relevant.

From chemistry point of view, molecular iodine has been extremely useful on the synthesis of various important organic compounds [16]. Molecular iodine is one of the most powerful catalysts used in laboratories. I_2 catalyzed reactions are used in the preparation of organic compounds. Essential organic chemical processes like catalyzation, protection and deprotection of carbonyl compounds, glycosylation reactions, condensed heterocycles, samarium-induced reactions, pyrrole synthesis, alkaloid synthesis, optically active polyaromatic alcohol, microwave-induced systems, etc. I_2 is being widely used. Description of these processes and the effect of I_2 on these reactions can be found in [16].

Because of its high reactivity, molecular iodine naturally exists in salt form [10]. Atomic iodine, which is very useful in many of the applied fields, are produced through the dissociation of I_2 molecule. Dissociation of I_2 molecule happens primarily through electron collision, photo-dissociation, and thermal vibronic motions. The electron collision studies with I_2 molecule has its own significance. Modelling of I_2 assisted chemical reactions requires knowledge of rate co-efficients, which are computed using the various elastic and inelastic cross-sections. Moreover, the DEA study is important for the understanding of chemical processes involving atomic anions. Keeping in mind the atmospheric science, iodine has an important role to play. The influence of iodine chemistry is higher compared to other halogen molecules. Halogen compounds are a potential threat to the tropospheric ozone [3]. The intermediate state of reaction with water molecule, iodine (I_2) forms an acidic environment, i.e. iodine on reaction with water forms HOI molecule, which is a volatile and carrier of radioiodine species (^{131}I) [4, 5, 6]. A detailed analysis on this can be found in [3].

Iodine is also special with reference to the complexity involved in the number of electrons present in the valance shell. The complexity is due to quantum theory, which shows a large number of valence-shell electronic states, mostly at higher energies, in Rydberg states [17, 18]. Watanabe [17] and Mulliken [18] have addressed the complexity involved in the study of I_2 molecule based on the potential scattering. In the present study, we performed an electron impact theoretical scattering calculation with iodine molecule and computed various cross-sections arising due to their interactions. The literature survey shows that electron impact cross-sectional studies for iodine molecules are sparse. Mulliken in his study [18] reported few of the excited states of the iodine molecule. The electronically excited states were experimentally reported by Huber and Herzberg [19] and Benjamine et al. [13]. Biondi and Fox in 1958 [20] reported theoretical data on dissociative electron attachment (DEA) cross-sections. While the experimental data on this was reported by Buchdhal in 1941 [21] and Healy in 1938 [22]. Buchdhal [21] measured these cross sections using ionization tube method while Healy's [22] results were based on swarm experiment. Both of these results were not accurate enough and found to be largely mismatching. The ionization cross-sections are theoretically studied by Joshipura and Limbachiya[23], Probst et al. [24], and Deutsch [25] under different theoretical approximations. The main motivation behind this work is to fill up the gap in the existing cross-sectional data on electron interaction, especially at low energies, looking to the wide range of applications [4, 5, 10, 11, 12, 13, 14, 15, 16] of I_2 molecule.

Thus, we report in this paper the electron impact scattering cross-sections, e.g. elastic, differential, momentum transfer, electronic excitations, DEA, and total cross sections for I_2 for incident electron energies ranging from 0.01 eV to 20 eV. We also report the ionization cross-section from its ionization threshold (9.307 eV) to 5000 eV.

2. Theoretical Methodology

We performed our scattering calculations using a fixed-nucleus approach, i.e. keeping the nucleus fixed at ground level in the molecular balance geometry via Quantemol-N [27]. Quantemol-N [27], a computing software for electron-molecule collisions, which uses the UK molecular R-matrix (UK-Rmol) code [28]. The R-matrix theory has been quite successful in predicting accurate electron scattering data for many molecules. Electron impact cross-section data for variety of molecules have been provided by our group [29, 31, 32] using the R-matrix method via Quantemol-N [27]. The mathematical uncertainty involved here depends on the assumptions taken for the calculations, and a detailed discussion regarding this can be found in the article provided by H-K Chung [26]. A detailed description of the R-matrix (Quantemol-N) can be found in our previous publications [29, 31, 32]. Nevertheless, we offer a brief description of the theoretical approach adopted here for the benefit of the new researchers.

The basic idea behind the R-matrix method [28, 33, 34] is to divide the complete configuration space into two spatial regions, separated by a sphere of radius 10 au $\sim$ 15 au (inner region) and 15 au $\sim$ 100 au (outer region) respectively which are centered at the center of mass of the molecular system.

2.1. Inner region

The inner region includes short-range potentials resulting from electron-electron interaction and exchange effects. All of these potentials play a crucial role in the description of electron target interaction and are resolved using quantum chemistry codes [28, 35, 36, 37]. Therefore, the boundary condition applied on the target wave function is that it must vanish at the inner boundary of the R-matrix. Here, we have assumed that it has zero amplitude on R-matrix boundary. To begin the computation, a trial wave function is generated for the inner region that has the form,

$$\Psi_k^{N+1}(x_1...x_{N+1}) = A\sum_{ij} a_{ijk}\Phi_i^N(x_1...x_N)u_{ij}(x_{N+1}) + \sum_i b_{ik}\chi_i^{N+1}(x_1...x_{N+1}) \quad (1)$$

The wave function obeys Pauli's exclusion principle, and this is taken care by anti-symmetrization operator A which makes the total wavefunction antisymmetric. The wave function of i^{th} target electronic state is represented by Φ_i, and the scattering electron is represented through continuum orbitals u_{ij}. The $N+1$ Hamiltonian matrix is diagonalized in order to get the values of variational parameters a_{ijk} and b_{ik}. The summation in the second term is carried out over χ_i for target plus scattering $(N+1)$ electrons, and it specifies L^2 function with the significance of zero amplitude at the R-matrix boundary. The expression for continuum orbitals is given by Faure et al. [38].

2.1.1. Scattering model

In this work, we have used the Static Exchange Plus Polarizations (SEP) and Configuration Interaction (CI) models via Quantemol-N [27] system. At the SEP level, only the target ground state wavefunction is used in the expression 1, so the resonance positions are described in a comparatively better manner than that of the CI method. In the CI method, a number of target electronic excited states are included in the expansion of the expression 1, which helps in detailing the information on the resonance status. These are normally described at the Complete Active Space (CAS) level, where the scattering electrons are allowed to occupy either an orbital in the active space or a virtual space.

For SEP and CI model calculations, we have used 3-21G basis set for the target wave function representation. The Hartree-Fock electronic configuration for the ground state (X^1A_g) $(X^1\sigma_g^+)$ of I_2 at its equilibrium geometry in D_{2h} point group symmetry is $1(a_g)^2$, $1(b_{1u})^2$, $2(b_{1u})^2$, $2(a_g)^2$, $3(a_g)^2$, $3(b_{1u})^2$, $1(b_{2g})^2$, $1(b_{3g})^2$, $1(b_{3u})^2$, $1(b_{2u})^2$, $4(a_g)^2$, $4(b_{1u})^2$, $5(a_g)^2$, $5(b_{1u})^2$, $2(b_{2g})^2$, $2(b_{3g})^2$, $2(b_{3u})^2$, $2(b_{2u})^2$, $6(b_{1u})^2$, $6(a_g)^2$, $3(b_{2g})^2$, $3(b_{3g})^2$,

$3(b_{3u})^2$, $3(b_{2u})^2$, $1(a_u)^2$, $7(b_{1u})^2$, $1(b_{1g})^2$, $7(a_g)^2$, $8(a_g)^2$, $8(b_1u)^2$, $9(a_g)^2$, $9(b_{1u})^2$, $4(b_{3u})^2$, $4(b_{2u})^2$, $4(b_{2g})^2$, $4(b_{3g})^2$, $10(a_g)^2$, $10(b_{1u})^2$, $5(b_{3u})^2$, $5(b_{2u})^2$, $5(b_{2g})^2$, $5(b_{3g})^2$, $2(b_{1g})^2$, $11(a_g)^2$, $2(a_u)^2$, $11(b_{1u})^2$, $12(a_g)^2$, $12(b_{1u})^2$, $13(a_g)^2$, $6(b_{3u})^2$, $6(b_{2u})^2$, $6(b_{3g})^2$, $6(b_{2g})^2$. All electrons are frozen in the lowest configuration in the SEP model. Among the total of 44 virtual orbitals included in the calculations, 10 virtual molecular orbitals (MOs) are of A_g symmetry, 5 virtual MOs of B_3u symmetry, 5 virtual MOs of B_2u symmetry, 2 virtual MOs of B_{1g} symmetry, 10 virtual MOs of B_{1u} symmetry, 5 virtual MOs of B_{2g} symmetry, 5 virtual MOs of B_{3g} symmetry and 2 virtual MOs of A_u symmetry are used for enhancement to the continuum orbitals. While in the case of configuration interaction (CI) model, out of 106 electrons, we have frozen 102 electrons in molecular orbitals $1a_g$, $2a_g$, $3a_g$, $4a_g$, $5a_g$, $6a_g$, $7a_g$, $8a_g$, $9a_g$, $10a_g$, $11a_g$, $12a_g$, $13a_g$, $1b_{3u}$, $2b_{3u}$, $3b_{3u}$, $4b_{3u}$, $5b_{3u}$, $6b_{3u}$, $1b_{2u}$, $2b_{2u}$, $3b_{2u}$, $4b_{2u}$, $5b_{2u}$, $6b_{2u}$, $1b_{1g}$, $2b_{1g}$, $1b_{1u}$, $2b_{1u}$, $3b_{1u}$, $4b_{1u}$, $5b_{1u}$, $6b_{1u}$, $7b_{1u}$, $8b_{1u}$, $9b_{1u}$, $10b_{1u}$, $11b_{1u}$, $12b_{1u}$, $1b_{2g}$, $2b_{2g}$, $3b_{2g}$, $4b_{2g}$, $5b_{2g}$, $1b_{3g}$, $2b_{3g}$, $3b_{3g}$, $4b_{3g}$, $5b_{3g}$, $1a_u$, $2a_u$. The rest of the 4 electrons were allowed to move freely in the active space of nine target occupied and virtual molecular orbitals $14a_g$, $15a_g$, $16a_g$, $7b_{3u}$, $7b_{2u}$, $13b_{1u}$, $14b_{1u}$, $6b_{2g}$, $6b_{3g}$. Eight virtual molecular orbitals (one of A_g symmetry, one of B_{3u} symmetry, one of B_{2u} symmetry, zero of B_{1g} symmetry, one of B_{1u} symmetry, one of B_2g symmetry, one of B_{3g} symmetry and zero of A_u symmetry) are used to enhance the continuum orbitals. A total of 47 target states are included in the close-coupling calculation involving 1194 configuration state functions for the ground state, and the number of channels included in the calculation are 135.

The R-matrix inner-region modules GAUSPROP and DENPROP generate target properties using Hartree-Fock calculations and construct the transition density matrix from the target eigenvectors obtained from CI calculations [27]. The multipole transition moments obtained are then used to solve the outer-region coupled equations. These are computed with the aid of second-order perturbation theory, and GAUSPROP evaluates the property integrals.

2.2. Outer region

The outer region calculations are simpler and hence less time-consuming. The main reason behind it is that scattering electron is distinguishable, and hence electron-electron correlation and exchange effects which make the calculations at the inner region complex are neglected. The interaction potential developed between the scattering electron and the target molecule is well approximated by considering single centre multipole potential expansion. In order to include the asymptotic solution in the outer region, the R-matrix is extended to the boundary by using the expression suggested by Gailitis [42]. The K-matrix so obtained is important as it contains all the information on the different observables. By diagonalizing K-matrix, we get the eigenphases, but one needs to retain the whole K-matrix to obtain all physical quantities that are necessary for the calculation of various cross-sections. The position and width data of the resonances are contained

in the eigen phase sum, which are deduced by fitting them to the Breit Wigner model. This task is performed by the RESON program [43]. We can easily deduce the transition matrix from the K-matrix using a simple relationship [28],

$$T = \frac{2iK}{1 - iK} \tag{2}$$

The other important cross-section that gives detailed information on the interaction between the target and the scattering electron is the differential cross-section (DCS). The various structures present in the DCS curve gives the signature of different low energy inelastic phenomena such as electronic excitation, dissociation, etc. The DCS is mathematically expressed as,

$$\frac{d\sigma}{d\Omega} = \sum_l A_l P_l(cos\theta) \tag{3}$$

where the solid angle is defined by Ω and the integral cross-section by σ. The Legendre polynomial of order l is represented by $P_l(cos\theta)$. Sanna and Gianturco [44] have given detailed knowledge on the coefficients, A_l and are therefore not replicated here. The momentum transfer cross-section (MTCS) is easily achieved by integrating the DCS with a factor of (1-cosθ).

2.3. Dissociative electron attachment (DEA)

Dissociative electron attachment (DEA) is one of the fundamental processes that occur at lower energy below the ionization limit. This phenomenon is closely related to the resonance process, i.e. the temporary capturing of the incoming electron and forms the transient negative ion (TNI) [45, 46]. The condition for the TNI formation as shown in figure 1. DEA contributes to the breakdown of molecules into neutral and anionic fragments by vibronic excitations, if not auto-detached. DEA thus becomes an important process for understanding the fundamental chemistry of the molecule in the presence of an extra electron such as

$$e^- + I_2(\Sigma_g^+) = I(^2P_{\frac{3}{2},\frac{1}{2}}) + I^-(^1S_0) \tag{4}$$

The total DEA cross-section $\sigma_T(E_i)$ is essentially the resonance cross sections $\sigma_r(E_i)$ arising from the formation of transient negative ion (TNI) and the survival probability of the resonant states 'S'. This TNI results through various resonance states and their corresponding survival rate. Thus the total DEA cross section $\sigma_T(E_i)$ can be expressed in the most simplified form as [47],

$$\sigma_T(E_i) = \sum_j C_j S_j \sigma_{rj}(E_i) \tag{5}$$

where E_i indicates the incident electron energy and the summation is made for the various resonances being considered. The coefficient C_j is the energy-dependent width

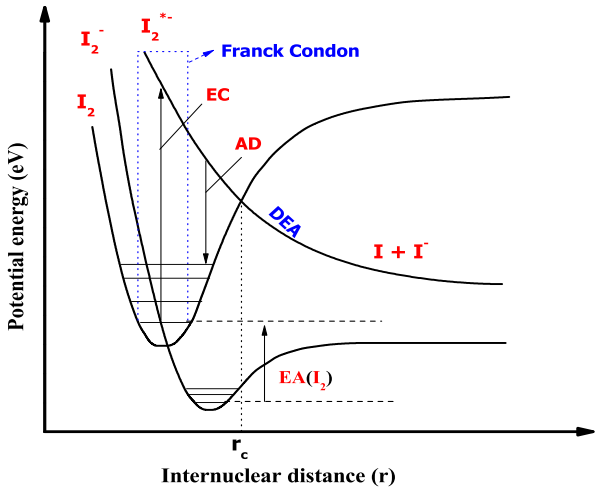

Figure 1. A pictorial representation of dissociative electron attachment (DEA) process of diatomic molecule (I_2). Here I_2 represents the neutral diatomic molecule, I_2^{*-} represents the excited diatomic molecule, I is the neutral fragmented atom, I^- represents the negative ion formed after fragmentation and EC is the Electron capture process for the Franck-Condon region, AD represents the Auto-detachment process and EA represents Electron affinity of the I_2 molecule.

of these resonances. When TNI persists beyond the $'r_c'$ crossing point (see Figure 1), then the target will disassociate into a neutral and anionic [48] component. More details of the DEA analysis can be found in our previous publications[29, 49].

The input parameter used for the DEA calculations are the dissociation energy of I^- from I_2, which is 1.58 eV [50], ground-state vibrational energy E_v of I_2, which is taken to be 1000 cm^{-1} as a standard frequency by Quantemol-N, and the electron affinity of iodine E_a, which is taken as 3.059 eV [51].

2.4. Ionization cross sections

The ionization of a molecule due to an electron impact is a very fundamental and important physical process during collisions. Electron impact ionization cross-sections have practical applications in many applied fields, e.g. fusion edge plasmas, fuel discharge plasmas, terrestrial, stellar and cometary atmospheres, radiation processing, mass spectrometry and in chemical analysis. Such wide applications of the ionization data have prompted many scientists around the world to focus on electron impact ionization of atoms and molecules to collect accurate Q_{ion} for critical scientific and industrial applications.

Kim and Inokuti [52] originally designed Binary-Encounter-Bethe (BEB) for the theoretical estimation of the ionization cross sections. The formula of the BEB method

to calculate ionization cross-sections is given as [52],

$$\sigma_{BEB} = \frac{S}{t+u+1}[\frac{lnt}{2}(1-\frac{1}{t^2})+1-\frac{1}{t}-\frac{lnt}{t+1}] \tag{6}$$

where t = $\frac{E_i}{B}$, u = $\frac{U}{B}$, S = $\frac{4\pi a_0^2 N R^2}{B^2}$, a_0 = 0.529 $\mathring{A}$ and R = 13.60 eV. Here E_i stands for incident energy, B for binding energy, U for kinetic energy and N for electron occupation number.

The BEB method is thus parameter-dependent, and the required data set for the calculation of ionization cross-sections involving the orbital kinetic and binding energies per symmetry are obtained from the Quantemol-N calculations. The parameter set for I_2 molecule is listed in the table 2. The estimated ionization cross sections using the BEB method is referred here as $Q_{ion(BEB)}$.

Another simple semi empirical method to compute ionization cross section is the Complex Scattering Potential-Ionization Contribution (CSP-ic) formalism. Details of this method can be found in many of our previous publications [29, 30], and it is used to calculate the ionization cross-sections in this case also. In this paper, we focus on the optical potential of the complex scattering potential of e-I_2 system and the foundation of the CSP-ic method involves the computation of the total inelastic cross sections Q_{inel} for energies beyond ionization threshold of the target. The optical potential adopted for the computation of Q_{inel} in the SCOP formalism is given by

$$V_{opt}(r, E_i) = V_R(r, E_i) + iV_I(r, E_i) \tag{7}$$

here E_i is the incident energy and the real part of the potential (V_R) includes the static, the exchange and the polarization effect. The imaginary part V_I is also referred to as the absorption potential V_{abs}, which accounts for the total loss of flux scattered across the two major inelastic channels, such as discrete electronic excitations or the continuum ionization channels. The well-known quasi-free model of Staszewska et al. [53, 54] with few modifications is used for the absorption part [55]. The final complex potential thus constructed is used to solve the Schrödinger equation numerically using the partial-wave method. The resulting phase shifts (δ_l) are used to determine the corresponding elastic (Q_{el}) and inelastic (Q_{inel}) cross-sections using the standard relations employing the scattering matrix, S_l(k) = exp $(2i\delta_l)$ [56]. Under the fixed nuclear approximation the total inelastic cross-sections contains two parts, (1) due to total discrete electronic excitations, (2) due to continuum ionization. Thus, the total inelastic cross-section is written as

$$Q_{inel}(E_i) = Q_{ion}(E_i) + \sum Q_{exc}(E_i) \tag{8}$$

The first term represents the total ionization, while the second term is the sum over all the electronic excitation cross sections for all accessible discrete transitions. By definition [57, 58, 59],

$$Q_{inel}(E_i) \geq Q_{ion}(E_i) \tag{9}$$

This is a fundamental inequality and it forms the roots for the Complex scattering potential-ionization contribution (CSP-ic) method [57, 58, 59]. The ionization cross-section may be estimated from the total inelastic cross section by defining an energy-dependent ratio $R(E_i)$,

$$R(E_i) = \frac{Q_{ion}(E_i)}{Q_{inel}(E_i)} \tag{10}$$

And it takes the value $0 \leq R \leq 1$ for any chosen value of E_i. The details of the CSP-ic method and the physical boundary conditions for the determination of this ratio and extraction of the ionization cross sections are well explained in our earlier publications [57, 58, 59] and hence skipped here. The ionization cross sections estimated using CSP-ic method is referred here as $Q_{ion(CSP-ic)}$ to differentiate it from that estimated using BEB method.

2.5. Total cross sections

Total electron scattering cross-sections for molecules are important for the study of electron transport properties in gases. They define the mean free path of electrons in the medium and, since they are the sum of all possible collision processes, constitute a valuable set of reference data. The total scattering cross sections is obtained by adding the total elastic and inelastic cross sections. The total inelastic cross sections in the present case consists of the cross sections resulting from DEA process, electronic excitation and ionization. As the ionization cross sections are estimated using the BEB method and using CSP-ic method, the total cross section computed here are indicated separately as $Q_{TCS(BEB)}$ and $Q_{TCS(CSP-ic)}$ respectively. Thus,

$$Q_{TCS(CSP-ic)} = Q_{el} + Q_{DEA} + Q_{exc} + Q_{ion(CSP-ic)} \tag{11}$$

$$Q_{TCS(BEB)} = Q_{el} + Q_{DEA} + Q_{exc} + Q_{ion(BEB)} \tag{12}$$

The $Q_{TCS(CSP-ic)}$ and $Q_{TCS(BEB)}$ are separately plotted in figure 9 for comparison.

2.6. Rate Co-efficient

The rate coefficient signifies the speed of any chemical reaction. Now in order to compute the rate coefficients [60], we use elastic and inelastic cross sections (see figure 7 & 8) as important input in the rate coefficient equation given below,

$$K_i = \left(\frac{8}{m_e\pi}\right)^{\frac{1}{2}} \left(\frac{1}{k_B T_e}\right)^{\frac{3}{2}} \times \int_0^\infty E_i Q^n(E_i) exp\left(-\frac{E_i}{k_B T_e}\right) dE. \tag{13}$$

Here mass of electron m_e, Boltzmann's constant k_B and electron temperature T_e are constant quantities. The rate coefficient is a function of the energy of incident electron E_i the ambient electron temperature T_e and the relevant cross-section $Q(E_i)$. The equation computes rate coefficient for two types of cross-sections. If $n > 0$, it signifies the rate coefficient for inelastic cross-sections which includes electronic excitation cross-sections and ionization cross-sections. If $n = 0$, then it corresponds to the rate coefficient for elastic scattering cross-sections. The rate coefficients are computed for wide electron temperature range from 100 ^oK to 10000 ^oK.

3. Results and Discussion

Table 1. Resonance position and width obtained fitting Breit Wigner model [43].

Sr. No.	State	Position (eV)	Width (eV)
1	$^2\Sigma_g^+$	8.3	$0.148*10^{+1}$
2	$^2\Pi_u$	4.53	$0.300*10^{+1}$
		6.36	$0.797*10^{+1}$
3	$^2\Sigma_g^-$	3.44	$0.461*10^{+1}$
		4.03	$0.900*10^{+1}$
		8.37	$0.133*10^{+1}$
4	$^2\Pi_g$	2.1	$0.158*10^{+1}$
5	$^2\Sigma_u^-$	6.38	$0.759*10^{+1}$

In the present study, we have computed electron impact cross-sectional data with the Iodine molecule (I_2), in the low-energy region using the Quantemol-N code. The cross-section data reported here are decomposition of elastic symmetric cross-sections in $D_{\infty h}$, differential cross-sections (DCS), momentum transfer cross-sections (MTCS), eigen phase sum, resonances, total elastic cross-sections, dissociative electron attachment (DEA), electronic excitations and ionization cross-sections (via CSP-ic method and BEB method separately). The I_2 molecule belongs to the $D_{\infty h}$ point group and we used the D_{2h} point group to solve the scattering problem as the Quantemol-N only provides abelian point group symmetries. The D_{2h} symmetric components have been set to $D_{\infty h}$ [50] using the following form, Σ_g^+ (A_g) ,Σ_u^+ (B_{1u}),Σ_g^- (B_{1g}), Σ_u^- (A_u), Π_u (B_{3u}, B_{2u}), Π_g (B_{3g}, B_{2g}), Δ_g (B_{1g}, A_g), Δ_u (A_u, B_{1u}).

In figure 2, we present the component wise elastic cross sections. The main focus of the presentation of symmetric cross-section information is to point out the resonance at each symmetric level. The peaks in the cross-section represents the particular physical process occurring at that particular energy and can be correlated with the transient resonance processes.

Table 2. Molecular orbitals (MO), electron binding energy B in eV, kinetic energy U in eV, and electron occupation number N used in BEB formalism to calculate the Ionizations

MOs	N	B	U	MOs	N	B	U
a_g	2	4617.90	7898.37	b_{1u}	2	4922.48	7891.07
a_g	2	1032.72	2362.18	b_{1u}	2	4617.90	7898.37
a_g	2	901.80	2319.54	b_{1u}	2	1032.72	2362.18
a_g	2	661.91	2167.39	b_{1u}	2	901.80	2319.55
a_g	2	661.71	2167.75	b_{1u}	2	661.91	2167.38
a_g	2	197.77	649.39	b_{1u}	2	661.71	2167.75
a_g	2	149.75	592.16	b_{1u}	2	197.77	649.44
a_g	2	66.09	448.44	b_{1u}	2	149.75	592.46
a_g	2	65.41	451.34	b_{1u}	2	65.97	451.45
a_g	2	24.91	87.99	b_{1u}	2	65.41	451.42
a_g	2	12.80	72.18	b_{1u}	2	21.51	101.51
b_{3u}, b_{2u}	2	4617.87	7898.63	b_{2g}, b_{3g}	2	4617.87	7898.63
b_{3u}, b_{2u}	2	901.64	2320.38	b_{2g}, b_{3g}	2	901.64	2320.37
b_{3u}, b_{2u}	2	661.86	2167.47	b_{2g}, b_{3g}	2	661.86	2167.47
b_{3u}, b_{2u}	2	149.36	595.09	b_{2g}, b_{3g}	2	149.35	595.11
b_{3u}, b_{2u}	2	65.88	450.04	b_{2g}, b_{3g}	2	65.84	451.06
b_{3u}, b_{2u}	2	11.99	64.29	b_{2g}, b_{3g}	2	9.93	73.30
b_{1g}	2	661.71	2167.75	a_u	2	661.71	2167.75
b_{1g}	2	65.41	451.34	a_u	2	65.41	451.42

Table 3. Vertical electronic energies from ground state of I_2 to various excited states and compared with available data reported [13, 18, 19]

State	Present (eV)	Theo. (eV) [18]	Experimental (eV)	State	Present (eV)
$1\ ^1\Sigma_g^+$	0	0		$1\ ^3\Sigma_u^+$	12.25
$1\ ^3\Pi_u$	2.18	2.37	1.25 [19], 1.95 [13]	$1\ ^3\Sigma_u^-$	12.52
$1\ ^1\Pi_u$	2.99	2.38		$2\ ^3\Pi_u$	12.52
$1\ ^3\Sigma_g^-$	5.44	3.9	5.04 [13]	$2\ ^1\Pi_u$	12.79
$1\ ^1\Delta_g$	6.26	4.4		$1\ ^1\Delta_u$	12.79
$2\ ^1\Sigma_g^+$	6.8			$2\ ^3\Sigma_u^-$	12.79
$1\ ^3\Pi_g$	10.88	8.1	5.13 [19, 13]	$2\ ^1\Sigma_u^-$	12.79
$1\ ^1\Pi_g$	11.16			$2\ ^3\Pi_g$	13.33

In figure 3, we show the electron impact eigen phase sum of the iodine molecule. It is primarily used to identify the resonances in the scattering system. The sudden change in the eigen phase sum at a particular energy represents the position of the resonance. The resonance observed in the cross-section data of $^2\Sigma_g^+$ and in eigen phase sum are almost identical at the same energy position in both the SEP and CI models. The resonance

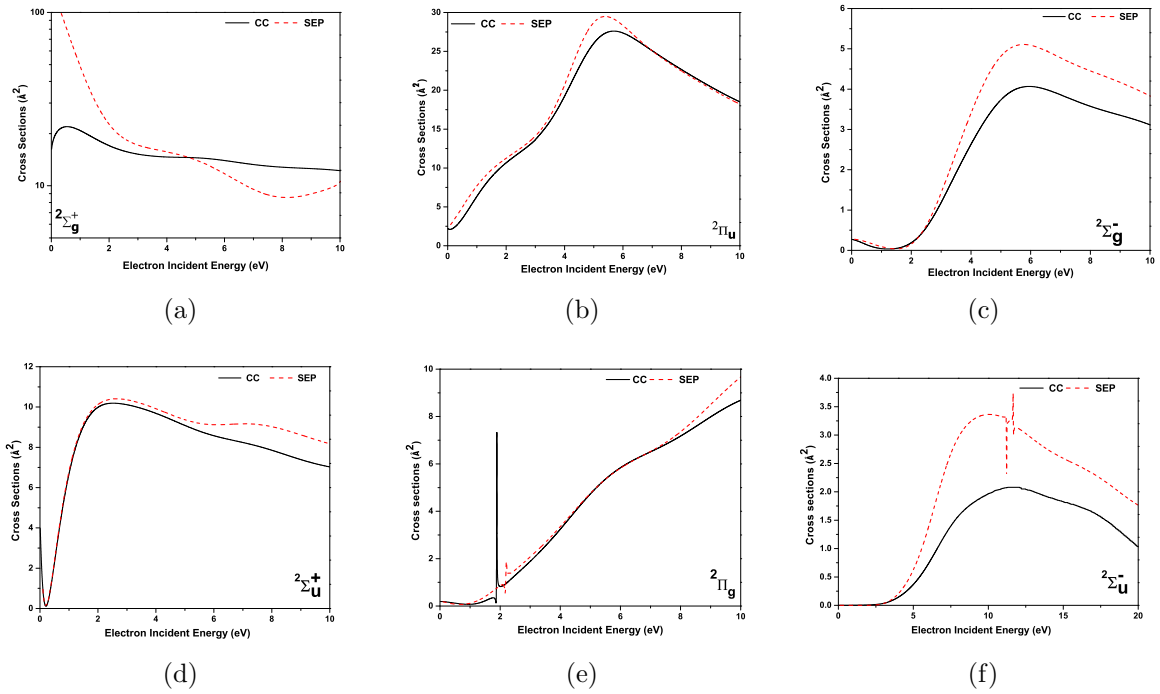

Figure 2. Decomposition of elastic cross sections in its symmetric components, where the solid line represents the CI model and dash line represents the SEP model calculated symmetric component of D_{2h} point group

at 8.24 eV is clearly visible in the eigen phase sum of the CI model, but a slight spike is seen in the elastic cross-section data of $^2\Sigma_g^+$ as observed in figure 2 (a). In the case of SEP model, we obtained no resonances below the ionization potential (I. P.) of the I_2 molecule, i.e. below 9.307 eV. This is clearly reflected in the elastic cross-section for the $^2\Sigma_g^+$ from the SEP model of figure 2 (a).

The $^2\Pi_u$ state plays a vital role in the dissociation of I_2 molecule. In the case of $^2\Pi_u$, the symmetric state resonance is observed at 6.91 eV as seen from the respective eigenphase sum obtained from the CI model of figure 3 (b). It is also observed in the corresponding symmetric state elastic cross sections shown in figure 2(b) at around 6 eV. The resonance parameters are then obtained by fitting them to Breit Wigner resonance formula [43]. In the case of SEP model calculations, the resonance at 4.53 eV is part of a shape resonance. In the case of $^2\Sigma_g^-$ symmetric state, a very strong resonance is obtained at around 2.10 eV, which is a part of a Feshbach resonace. The resonance position and with obtained by fitting the eigenphase sum to Briet Wigner formula are listed in table 1

The analysis of DCSs for any scattering theory is a rigorous test as it is sensitive to results that are commonly averaged out in the integral cross-sections. In figure 4, we present the DCS computed using the CI model. As there are no DCS data available

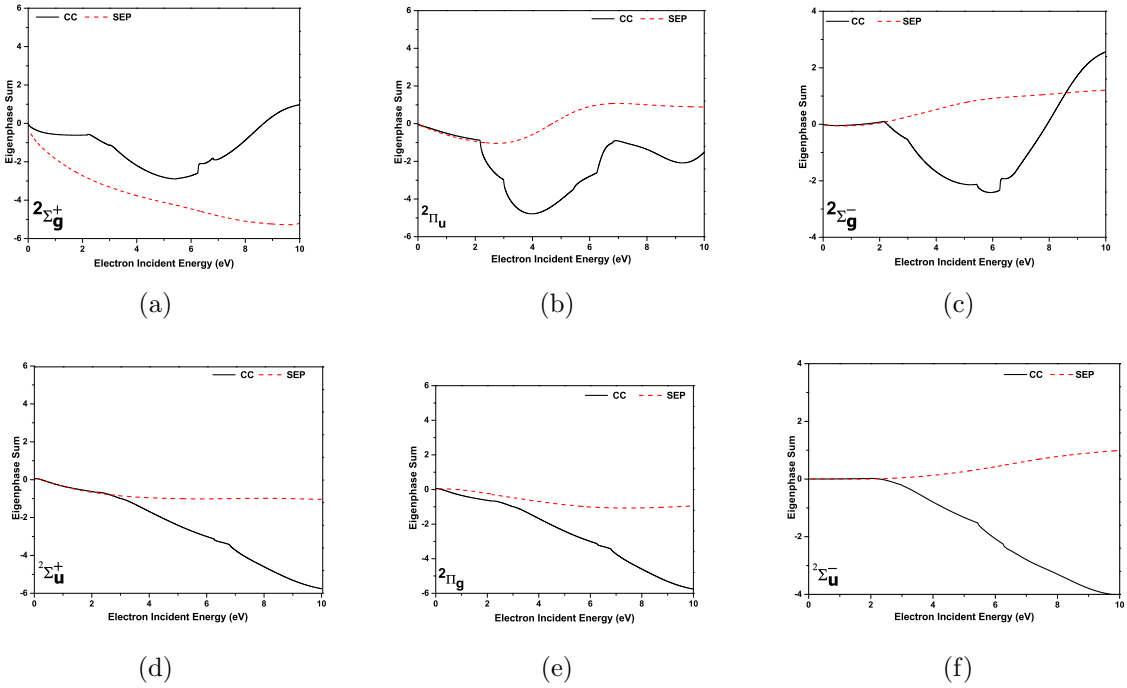

Figure 3. Eigenphsae for the resonance, where the solid line represents the CI model calculated symmetric component and dash line represents the SEP model calculated symmetric component

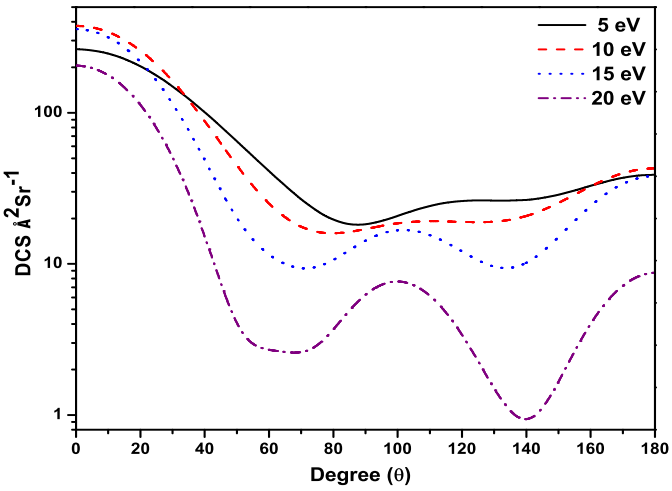

Figure 4. Differential cross sections (DCS), where solid line represents 5 eV, dash line represent 10 eV, dot line represents 15 eV and dash dot line represents 20 eV.

in literature on the iodine molecule, the present attempt may be the first effort of documentinng DCS results of $e - I_2$ scattering. DCS curves for incident energies 5 eV, 10 eV, 15 eV and 20 eV are shown in figure 4. The two prominent features observed in the DCS curve get enhanced as energy increases from 5 eV to 20 eV. These dips arise from cancellations of attractive and repulsive potentials leading to very low scattering

amplitudes and hence low values of the DCS.

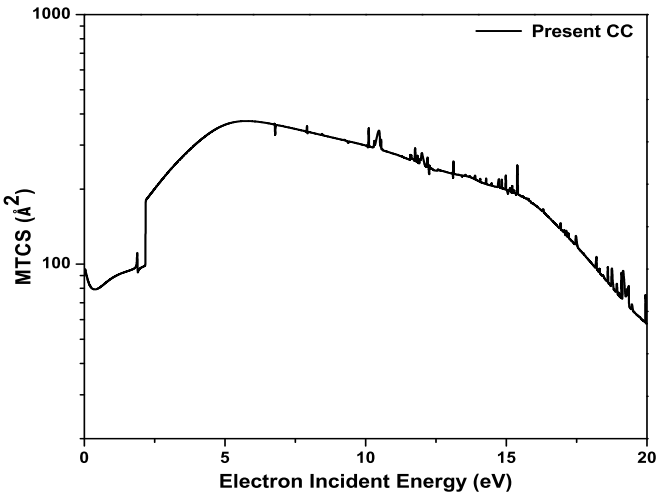

Figure 5. Momentum transfer cross sections, where the solid line represent the present calculated result.

In Figure 5, we show the momentum transfer cross-section (MTCS) which is integrated differential cross-section with the parameter (1-cosθ). The MTCS related study is significant as it demonstrates the importance of the backward scattering and is an important quantity to solve the Boltzmann equation for the swarm of electrons and their drift velocity in the molecular gas. The resonance predicted in the CI model is also explicitly seen in the MTCS curve. Many peaks seen beyond the 12 eV energy corresponds to the complexity related to the electron configuration of the I_2 molecule. The properties of the MTCS curve and the resonances of the symmetrical decomposition of the elastic cross-sections complement to each other. The sudden increase at 2.18 eV in the MTCS is associated with the electronically excited Feshbach resonance of the first excited state ($^3\Pi u$) as discussed earlier.

On dissociative electron attachment process, the I_2 molecule gives a neutral and anionic atomic state, as per equation 4. The present DEA cross-sections using the CI and SEP target models provided by Quantemol-N are plotted in figure 6. The DEA cross-section using the SEP model is on the lower side compared to that of the CI model. This difference between them may be attributed to the difference in the position and width of the resonances provided by these two models. In the DEA cross-sections, we observed two different peaks one at 1.58 eV with cross-sections of 0.121 $\AA^2$ and other at 10.8 eV with a cross-section of 0.802 $\AA^2$ using the CI model. The first peak appears at the bond dissociation energy of I_2. The second peak is due to π state shape resonance. In the SEP model these two peaks are shifted little at 1.8 eV with a cross-section of 0.055 $\AA^2$ and at 11.58 eV with cross-sections of 0.335 $\AA^2$. The present result is found to

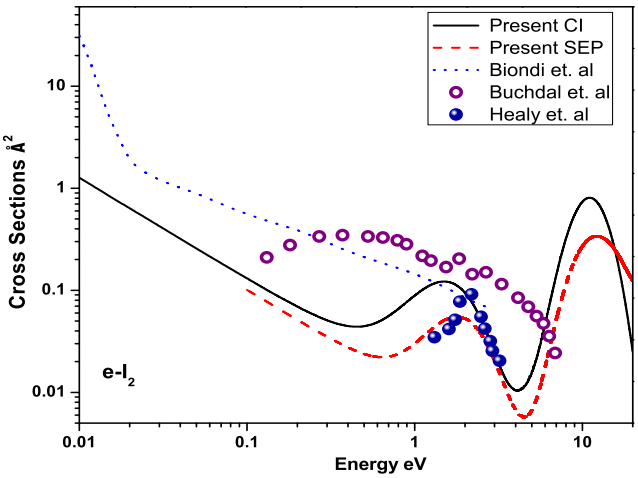

Figure 6. Dissociative electron attachment cross-sections, where the solid line represents the present calculated data using CI model, dash line represents the present calculated data using the SEP model, dot line represents the calculated data by Biondi et al. [20], the circle represents the measured data by Buchdal et al. [21], and the solid sphere represents the measured data by Healy et al. [22].

be in better agreement with the measurement of Healy [22] for the energy 2 eV to 4 eV. The monotonically decreasing trend of DEA cross-sectons of the present case at very low energy resembles that of Biondi and Fox [20]. It is to be noted that the first peak observed in the energy range 1 eV to 2 eV is also observed in the experimental results of both Healy [22] and Buchdhal [21]. The shift in the peak position in the experiment data of Buchdhal [21] may be due to the procedure of averaging over the electron energy distribution used in the analysis of their measurements.

The inelastic channel at the low energy under the fixed nuclei assumption is dominated by the discrete electronic excitations (Figure. 7(a)). In figure 7(a), we show the electronic excitation cross-sections of $e - I_2$ scattering. The present result is a partial electronic excitation cross-section calculated for point group D_{2h} using a basis set 3-21G. The solid line (violet colour line) represents the total electronic excitation cross-sections below 20 eV for the first time to the best of our knowledge. The calculated, vertical excited state of I_2 molecule is reported in table 3. The present results are in overall good agreement with the available data in literature [18, 13, 19]. The reported data shows degeneracy in the higher electronic excited state; the reason behind this is the use of lower point group symmetry D_{2h}. This degeneracy can further be removed on using the higher point group symmetry such as D_{6h}. However, in the absence of reliable data and considering the complexity involved, the estimations provided in this study are useful.

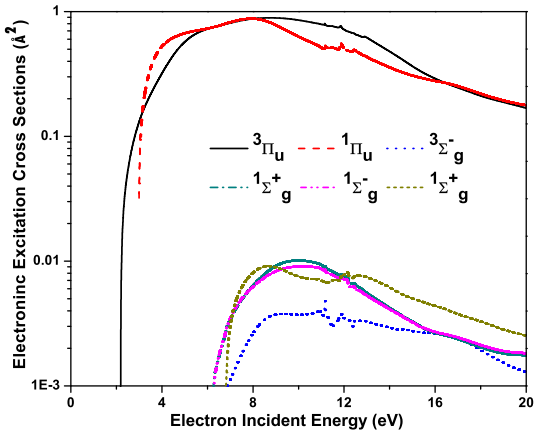

(a)

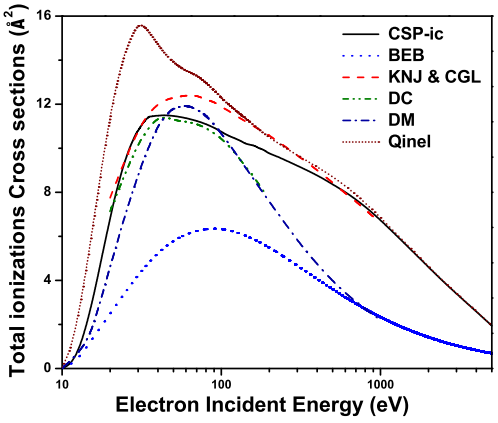

(b)

Figure 7. Absorbtion channel, where in fig.(a) we present the partially calculated electronic excitation cross sections using the Quantemol-N (where solid line represent $^3\Pi_u$, dash line $^1\Pi_u$. dot line $^3\Sigma_g^-$, dash dot line $^1\Sigma_g^+$, dash dot dot line $^1\Sigma_g^-$ and short dash line $^1\Sigma_g^+$) and in fig.(b) we present the total ionization calculated using the CSP-ic formalism.

The other inelastic channel through which the incident flux gets lost in the continuum is the ionization. In figure 7 (b), we report the total ionization cross sections for $e - I_2$ scattering. The present results underestimate the calculated data by Joshipura and Limbachiya [23], but is in good agreement with the data of Deutsch-Marek (D.M.) [24] and that computed using Defect Concept (D.C.) by Deutsch et al. [25]. It is found that the variation observed in the CSP-ic data beyond 300 eV is due to the large total inelastic cross-section obtained through SCOP formalism. To illustrate this fact, we have included the total inelastic cross-section along with the ionization cross-section in figure 7 (b). The behaviour of inelastic cross-section beyond 300 eV has comparatively high values which are reflected in the ionization cross-section as the ionization cross-section is extracted from the total inelastic cross-sections using equation 8. The BEB

[52] results are low compared to all the other reported theoretical data.

The differences observed in the compared cross-sections are mainly related to various approximations involved in the theoretical approaches. In the present case, we have used a single-centre approach to justify partial wave analysis. The end product of this method is phase shift which is directly included for the production of inelastic cross-section and to the estimation of ionization cross sections using CSP-ic method. Joshipura and Limbachiya [23] in their study also employed the SCOP formalism and CSP-ic method to estimate the ionization cross sections but they have adopted the (I+I) additivity rule, which generally overestimates at low energies. The Binary-Encounter-Bethe (BEB) [52] and Deutsch-Mark (D.M.) [24] results are microscopic in nature in the sense that they are based on considerations involving individual molecular orbitals whereas the D.C. [25] is an alternate form of D.M. [24] formalism which is a modified additivity rule incorporating the defect concept. A detail description about the defect concept is available in [25]. However, the comparison between all these different approaches is meaningful in the absence of experimental data.

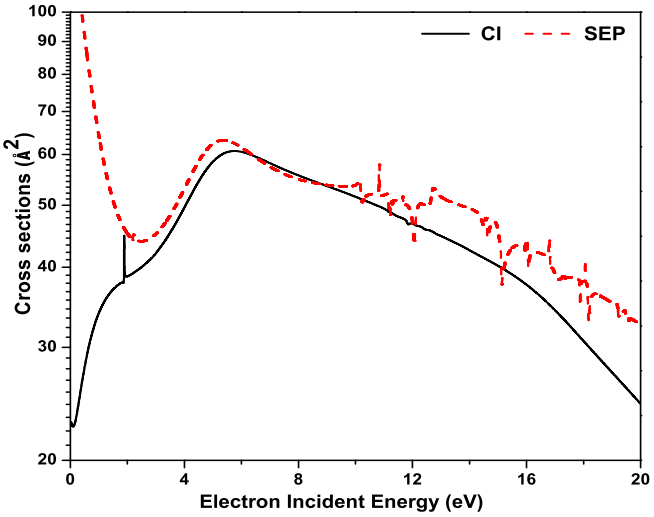

Figure 8. Total elastic cross sections, where the solid line represents calculated result using CI method and dash line represents the SEP calculated result.

The total sum of all the elastic and inelastic processes that take place between an incident electron and the target is given by total cross sections (TCS). Total cross-sections show the probability of occurrence of various phenomenon collectively. The features observed in TCS curve below 20 eV reflects the different prominent inelastic phenomena such as resonances, electronic excitation, DEA etc. Above 20 eV the significance of these resonances declines and no such features are observed in TCS. In figure 8, we report the calculated total elastic scattering cross sections using the CI model, and we also report the total elastic scattering cross sections using SEP model.

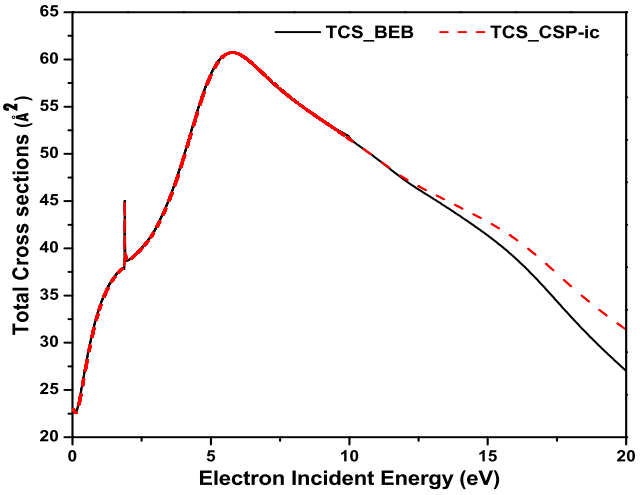

Figure 9. Total cross sections using the CI model, where the solid line represents calculated result using CSP-ic ionization included in TCS and dash line represents the BEB calculated ionization result included in TCS.

In the SEP model, the cross-sections at very low energy, i.e. below 2.5 eV are very high. Further, the resonance position is shifted in the SEP model compared to that of the CI model. The sharp rise in the cross-sectional value accounts for the formation of transitive negative ion (TNI). TNI is a resonant phenomenon which is visualized at specific energies and reveals themselves in the form of sharp peaks or troughs or a sudden rise in the interaction cross-sections. Thus, they are also designated as electron scattering resonances [61]. This helps us in understanding the DEA phenomena. And the reported value is relevant to the dissociation of the bond of I_2 molecule. The maximum rise in the cross-sectional value at 5.5 eV is 60.50 $\mathring{A}^2$.

In figure 9 we have represented the calculated total cross-section for the energy 0.1 eV to 20 eV. Beyond the ionization threshold (9.307 eV), the differences shown in figure 9 are the one that corresponds to the difference between the $Q_{ion(BEB)}$ and $Q_{ion(CSP-ic)}$.

Electron impact scattering rate coefficients are plotted (figure 10) as a function of the electron kinetic temperature defined through the Maxwell-Boltzmann distribution. At thermal equilibrium, the distribution of the electron energy is defined by the Maxwellian form and is a function of the gas temperature. Rate constants for elastic and inelastic processes are extracted from the born corrected R-matrix cross-sections. In the present case, these rate coefficients are important in understanding the reaction rates at the troposphere iodine chemistry [4, 5, 6]. A lot has been discussed regarding the reactivity of the iodine molecule and the formation of different compounds of iodine which are responsible for depletion in the tropospheric ozone layer. This cross-sectional study will definitely help in understanding the major reaction parts. The plasma-based modelling will definitely be benefited by the various cross-sectional data presented in this study.

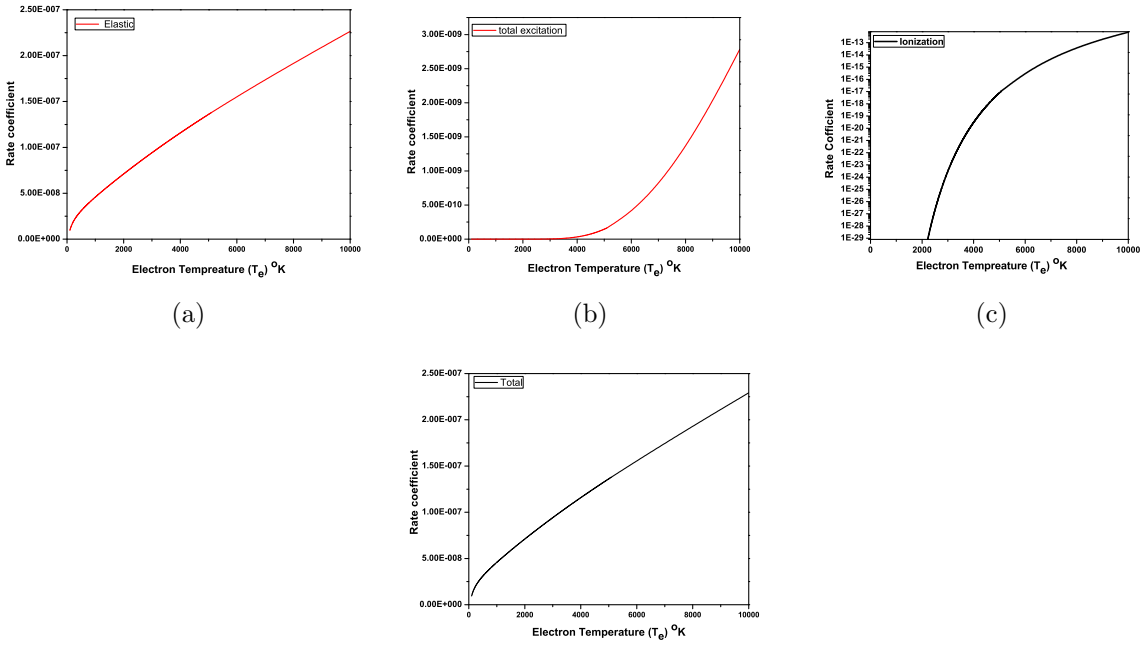

Figure 10. Rate coefficient vs Electron Temperature (T_e) using CI model, where in fig.(a) we present the rate coefficient of elastic scattering, in fig.(b) we present the rate coefficient of total electronic excitation scattering, in fig.(c) we present the rate coefficient of total ionization (BEB) scattering and in fig. (d) we present the total (elastic + total electronic excitations + ionization scattering).

4. Conclusion

In the present paper, we have computed the electron impact scattering cross-sectional data for iodine molecule (I_2) for impact energies ranging from 0.01 eV to 20 eV. This is the first attempt to provide the data on elastic, differential, momentum transfer, electronic excitation and total cross-section for electron impact on iodine molecule. The present DEA data find relatively in good agreement with experimental data of Healy [22] for the very limited energy range. From the results of elastic components and eigen phase sum, we have been able to identify many resonances correspond to different symmetric states. All these resonances are also been observed in our MTCS curve (see figure 5). It is important to note that electronically excited Feshbach resonance at 2.1 eV is an important finding of the present study. As halogen being one of the highly electronegative atoms, the experimental work becomes more difficult and, in that scenario, the theoretical prediction can be useful in many modelling studies related to iodine molecule.

Acknowledgement

Minaxi Vinodkumar acknowledge DST-SERB, New Delhi for the Major research project [EMR/2016/000470] for financial support under which part of this work is carried out. Authors are grateful to the referees for their constructive input.

References

[1] Scott A. Rivkees, Charles Sklar, and Michael Freemark, (1998) *The Journal of Clinical Endocrinology & Metabolism (JCEM)*, **83** (11): 376776.

[2] Greenwood N. N., Earnshaw A., 1997 *Chemistry of the Elements : 2nd Edition* (Butterworth-Heinemann/ELSEVIER) p 800.

[3] Saiz-Lopez A., Fernandez R. P., Ordez C., Kinnison D. E., Gmez Martn J. C., Lamarque J.F., and Tilmes S., 2014 *Atmos. Chem. Phys.*, **14**, 1311913143.

[4] Yadav H., Bhutadia H., Prajapati D., Desai H., Vinodkumar M. and Vinodkumar P. C., 2018 *AIP Conference Proceedings* **1953**, 140106 : doi: 10.1063/1.5033281.

[5] Jenkin M. E., Cox R. A., Candeland D. E., 1985 *J. Atmos. Chem.* **2**, 359.

[6] Chameidis W. L.,Davis D. D., 1980 *J. Geophys. Res.*, **8**, 7383.

[7] Carpenter L. J. , MacDonald S. M., Shaw M. D., Kumar R., Saunders R. W., Parthipan R., Wilson J. and Plane J. M. C., 2013 *Nature Geoscience*, **6**, 108111.

[8] Davis D., Crawford J., Liu S., McKeen S., Bandy A., Thomton D., Rowland F., and Blake D., 1996 *J. Geophysical Reserach*, **101**, 2135-2147.

[9] Simpson W. R., Brown S. S., Saiz-Lopez A., Thornton J. A.,and Glasow R, 2015 *Chem. Rev.*, **115**, 40354062.

[10] Johnson C C, 2003 *The geochemistry of iodine and its application to enviromental strategies for reducing the risks from iodine deficiency disorders.* Bristish Geological Survey Commissioned Report. CR/03/057N. 54pp.

[11] Shuaibov A.K., Minya A.I., Gomoki Z.T., Kalyuzhnaya A. G., and Shchedrin A. I., 2010 *Tech. Phys.*, **55**, 1222. https://doi.org/10.1134/S1063784210080232

[12] Shchedrin A. and Kalyuzhnaya A., (September 26th 2011). *Numerical Simulation of Plasma Kinetics in Low-Pressure Discharge in Mixtures of Helium and Xenon with Iodine Vapours, Numerical Simulations of Physical and Engineering Processes, Jan Awrejcewicz, IntechOpen*, DOI: 10.5772/24419.

[13] Prince B. D., Levandier D. J., and Bemish R. J., *Application of a First Generation Collisional Radiative Model for Iodine to Optical Emissions from the Plume of an Iodine Hall Effect Thruster* 53rd AIAA/SAE/ASEE Joint Propulsion Conference. July

[14] Maria Choi *MODELING AN IODINE HALL THRUSTER PLUME IN THE IODINE SATELLITE (ISAT)* NASA Glenn Research Center Cleveland, OH.

[15] Dietz P., Grtner W., Koch Q., Khler P. E., Teng Y., Schreiner P. R., Holste K. and Klar P. J., 2019, *Plasma Sources Sci. Technol.* **28**, 084001.

[16] Banik Bimal, (2017) *Mod Chem appl* 5 : 3.

[17] Watanabe K., 1975 *J. Chem. Phys.* **26**, 542; doi: 10.1063/1.1743340.

[18] Mulliken R. S., 1971 *J. Chem. Phys.* **55**, 288.

[19] K. Huber; Herzberg, G., 1979 *Molecular Spectra and Molecular Structure. IV. Constants of Diatomic Molecules.* Published by Van Nostrand ISBN 10: 0442233949 ISBN 13: 9780442233945, pp 332.

[20] Biondi M A and R E Fox, 1958 *Phys. Rev.*, **109**, 2012.

[21] Buchdal R J., 1941 *Chem. Phys*, **9**, 146.

[22] Healy R H , 1938 *Philos. Mag*, **26**, 940.

[23] Joshipura K N and Limbachiya C G, 2002 *Int. J. of Mass. Spect.* **216**, 239.
[24] M. Probst, H. Deutsch, K. Becker, T. D. Maerk, 2001 *Int. J. of Mass. Spect.*, **206**, 13.
[25] H. Deutsch, K. Becker, T. D. Maerk, 2000 *Euro. Phys. J. D.*, **12**, 283.
[26] Chung H. K., Braams B. J., Bartschat K., Csszr A. G., Drake G. W. F., Kirchner T., Kokoouline V. and Tennyson J., 2016 *J. Phys. D: Appl. Phys.*, **49**, 363002.
[27] Tennyson J, Brown D B, Munro J J, Rozum I, Varambhia H N and Vinci N, 2007 *J. Phys.: Conf. Ser.* **86** 012001.
[28] Tennyson J., 2010 *Physics Report* **491**,2, 29-76.
[29] Yadav H., Vinodkumar M., Limbachiya C. and Vinodkumar P.C., 2017 *Mol. Phys.*, **115**, 952.
[30] Prajapati D., Yadav H., Vinodkumar P. C., Limbachiya C., Dora A. and Vinodkumar M, 2018 *Eur. Phys. J. D.*, **72**, 210.
[31] Vinodkumar M., Desai H., Vinodkumar P. C. and Mason N., 2016 *Phys. Rev. A*, **93**, 012702.
[32] Limbachiya C., Chaudhari A., Desai H. and Vinodkumar M. 2015 *RSC Adv.*, 2015, 103964.
[33] BURKE P. G. , 1978 *J. Phys. Colloques* **39** C4-27.
[34] Burke P.G., Berrington K.A. (Eds.), 1993 *Atomic and Molecular Processes, an R-matrix Approach*, Institute of Physics Publishing, Bristol..
[35] Morgan L.A., Gillan C.J., Tennyson J., Chen X., 1997 *J. Phys. B: At. Mol. Opt. Phys.* **30**, 4087.
[36] Huo W.M., Brown D., 1999 *Phys. Rev. A* **60** 295.
[37] Kolorenc P., Cizek M., Horacek J., Milnikov G., Nakamura H., 2002 *Phys. Scr.* **65 328**.
[38] Faure A., Gorfinkiel J. D., Morgan L. A. and Tennyson J., 2002 *Comput. Phys. Commun.* **144**, 224.
[39] Chu S. I. and Dalgarno. A, 1974 *Phys. Rev. A*, **10**, 788.
[40] Itikawa Y., 1972 *J. Phys. Soc. Jpn.*, **32**, 217-226.
[41] Norcross D. W. and Padial N. T., 1982 *Phys. Rev. A*, **25**, 226.
[42] Gailitis M., 1976 *J. Phys. B: At. Mol. Phys.*, **9**, 843.
[43] Tennyson J. and Noble C. J.,1984 *Comput. Phys. Commun.*, **33**, 421.
[44] Sanna N., and Gianturco F.A., 1998 *Comput. Phys. Commun.*, **114**, 142.
[45] Thorman R M, Kumar R, Fairbrother H D and Inglfsson O,2015 *Beilstein J. Nanotechnol.* **6**, 1904.
[46] Christophorou, 1980 *Environmental Health Prespectives*, **36**, 3.
[47] Munro J. J. , Harrison S, Fujimoto M M and Tennyson J, 2012 *J. of Phys: Conference Series,* **388** 012013.
[48] Fabrikant I. I., 2010 *J. Phys. Conf. Ser.*, **204**, 012004.
[49] Yadav H., Vinodkumar M., Limbachiya C. and Vinodkumar P. C., 2018 *J. Phys. B: At., Mol. Opt. Phys.*, **51**, 045201.
[50] Gerhard Herzberg, 1996 *Molecular Spectra and Molecular Stracture Volume:3. Electronic Spectraand Electronic Structure of polyatomic Molecule* (D. VAN NOSTRAND COMPANY, Inc.) p 576.
[51] http://cccbdb.nist.gov.
[52] Kim Y. K. and Rudd M. E., 1994 *Phy. Rev. A*, **50**, 3954.
[53] Staszewska G.,Schwenke D. W. and Truhlar D. G., 1984 *J. Chem. Phys.* **81** 3078.
[54] Staszewska G., Schwenke D. W., Thirumalai D. and Truhlar D. G., 1984 *Phys. Rev. A* **29** 3078.
[55] M. Vinodkumar, K. Korot, and P.C. Vinodkumar, Eur. Phys. J. D 59, 379387 (2010).
[56] Joachain C J, 1983 *Quantum Collision Theory* (North-Holland Press, Amsterdam).
[57] Vinodkumar M, Limbachiya C, Barot M, Swadia M, Barot A, 2013 *Int. J. M. Spect.* **339340** 16.
[58] Vinodkumar M, Bhutadia H, Limbachiya C, Joshipura K N,2011 *Int. J. M. Spect.*, **308** 35.
[59] Vinodkumar M, Bhutadia H, Dave R and Antony B, 2011 *Inidian J. Phys.*, **85**, 1761.
[60] Singh J., Baluja K. L., Longiany G., 2017 *Pramana* **88**, 76.
[61] Schulz G J., 1973, *Rev. of Mod. Phys.* **45**, 378-486.